Morphological Behavior of Thermally Treated Polystyrene-*b*-polybutadiene-*b*-poly(ϵ-caprolactone) ABC Triblock Copolymers

V. Balsamo,*,† G. Gil,‡ C. Urbina de Navarro,‡ I. W. Hamley,§ F. von Gyldenfeldt,|| V. Abetz,|| and E. Cañizales†

Grupo de Polímeros USB, Departamento de Ciencia de los Materiales, Universidad Simón Bolívar, Aptdo. 89000, Baruta, Edo. Miranda 1080A, Caracas, Venezuela, Centro de Microscopía Electrónica, Universidad Central de Venezuela, Caracas, Venezuela, Department of Chemistry, University of Leeds, Leeds, U.K., and Makromolekulare Chemie II, Universität Bayreuth, D-95440 Bayreuth, Germany

Received January 25, 2002

ABSTRACT: The microphase morphology of a series of polystyrene-*b*-polybutadiene-*b*-poly(ϵ-caprolactone) ABC triblock copolymers (SBC) was studied by transmission electron microscopy (TEM) and synchrotron radiation small-angle X-ray scattering (SAXS) for selected samples. The studies were performed as a function of annealing time at high temperature (150 °C). Interestingly, even though crystallization took place under similar conditions (5 h at 40 °C), the annealing time at high temperature can influence the final morphology in such a way that within a copolymer ($S_{51}B_{09}C_{40}$), a morphological transition from a lamellar−cylindrical (lc) to a cylindrical−ring (cr) morphology can occur. It was also observed that the copolymers reach varied levels of long-range order of the microdomains, depending on the composition. These results combined with the observation or not of well-defined spherulites in the bulk illustrate the strong "conflict" between microphase separation and crystallization, especially when the PCL content is relatively high. The morphological changes are directly related to the thermal behavior of the triblock copolymers, in particular, the melting temperature and Avrami parameter associated with the crystallization kinetics.

Introduction

It has been recognized that the microphase morphology in semicrystalline block copolymers is strongly influenced by the competition between crystallization and microphase separation. This has been investigated for diblock copolymers by several groups.[1−15] When a block copolymer crystallizes from a homogeneous or a weakly segregated melt and both blocks are above their glass transition temperatures, the melt mesophase is generally destroyed upon crystallization, and a lamellar morphology and ultimately a spherulitic superstructure is adopted upon crystallization.[1−8] In contrast, even a weakly segregated mesophase can effectively confine the crystallizable block to nanometer-scaled domains if the noncrystallizable majority block is glassy at the crystallization temperature;[9−13] the same effect is observed by increasing segregation strength in a rubbery block copolymer.[14]

In the same way, the orientation of the crystalline stems can be influenced by the block copolymer mesophases. If crystallization determines the final microphase morphology, a perpendicular orientation of the chain axis with respect to the microdomain interfaces has been confirmed in lamellar microdomains.[1,2,7] In the case of crystallization in nanoconfined lamellae various crystal orientations have been observed experimentally for different block copolymers. For some poly(ethylene oxide)- (PEO-) containing diblock copolymers, a perpendicular orientation of the chain axis to the lamellar surface has been found.[16−20] On the other hand, for some shear-aligned polyethylene- (PE-) containing diblock copolymers a parallel orientation of the chain stems has been observed.[12,21] In the case of crystallization in confined cylinders, a perpendicular or slightly tilted orientation has also been proposed.[10] However, more recently, it has been demonstrated that for shear-aligned PEO-*b*-PS diblock copolymers the orientation depends on the crystallization temperature.[22,23]

Thus, the interplay between microphase separation and crystallization in semicrystalline diblock copolymers is a complicated function of crystallization temperature, segregation strength and physical state of the noncrystalline block. The situation is expected to be even more complex if crystallization takes place in an ABC triblock copolymer. To illustrate the richness and complexity of these systems, Balsamo et al.[24−26] demonstrated that when crystallization of the poly(ϵ-caprolactone) block is confined in cylinders in PS-*b*-PB-*b*-PCL triblock copolymers, it is able to deform the cylinders despite their location in a glassy matrix. Simultaneously, crystallization can occur in a fractionated fashion, with a combination of heterogeneous and homogeneous nucleation.[33] More recently, it has been demonstrated that such behavior is general for semicrystalline ABC triblock copolymers with one or two confined semicrystalline blocks.[27,28] On the other hand, when the crystallizable component is found in a relatively high quantity, spherulitic superstructures are formed.[29,30] In these cases, Balsamo et al. detected morphological transitions by changing the crystallization conditions.[29] Bates et al.[31] were able to determine the approximate phase diagram for intermediate to weakly segregated systems between symmetric PS-*b*-PI and PS-*b*-PI-*b*-PEO com-

* To whom correspondence should be addressed. E-mail: vbalsamo@usb.ve.
† Universidad Simón Bolívar.
‡ Universidad Central de Venezuela.
§ University of Leeds.
|| Universität Bayreuth.

10.1021/ma020129o CCC: $25.00
Published on Web 05/23/2003

Table 1. Molecular Characteristics of the Materials and Volume Fractions of the Components in the SBC Triblock Copolymers

copolymer[a]	ϕ_{PS}	ϕ_{PB}	ϕ_{PCL}[b]	$M_{n(cop)}$ (kg/mol)	$M_{n(PCL)}$ (kg/mol)	M_w/M_n
$S_{57}B_{27}C_{16}$	0.55	0.30	0.15	137	22	1.12
$S_{51}B_{09}C_{40}$	0.50	0.10	0.40	98	39	1.15
$S_{25}B_{26}C_{49}$	0.25	0.30	0.45	84	41	1.15
$S_{27}B_{15}C_{58}$	0.27	0.17	0.56	219	127	1.30

[a] Subscripts represent the weight percent of each component. [b] Calculated taking into account the degree of crystallinity.

positional states. Nevertheless, no investigation of the relationship between microphase separation and crystallization was given.

The reported results on the morphology and crystallization of PCL-based ABC triblock copolymers have led to the intriguing question of how spherulites can form in and break through a microphase-separated structure in which one of the components is glassy. In a first attempt to explain this effect, Jackson et al. reported that the formation of spherulites in a $S_{35}B_{15}C_{50}$ copolymer is strongly affected by the thickness of the specimen.[32] They observed, for example, that, in a $S_{35}B_{15}C_{50}$ copolymer, spherulite formation is only observed in thin films and that the order resulting from the microphase separation in the melt was partially destroyed, but when the same copolymer crystallized from the bulk, the microphase separation was preserved and no spherulite formation was observed.

In view of these investigations, we explore in this work the coexistence of microphase separation and superstructure formation in copolymers of varied composition and we try to relate the morphology with the thermal behavior of such copolymers, which has been previously investigated.[33] In that work, it was demonstrated that not only the crystallization conditions but also the time during which the sample was annealed can strongly affect the crystallization and, therefore, the melting behavior and crystallization kinetics.

Experimental Part

Materials. Table 1 shows the molecular characteristics of the polystyrene-*b*-polybutadiene-*b*-poly(ϵ-caprolactone) triblock copolymers used in the present study. These block copolymers were synthesized via sequential living anionic polymerization as described in an earlier work.[34] The absence of rests of homopolymers (PS and PCL) and diblock copolymer (PS-*b*-PB) was confirmed by GPC experiments

Polymer films (∼1 mm thick) were slowly cast from 5% w/v toluene solutions at room temperature. They were then placed in a vacuum oven at room temperature for 3 days to eliminate solvent traces. Samples of the films were subjected to a thermal treatment performed under nitrogen atmosphere. The thermal treatment was performed by holding the samples at 150 °C for 5 (TT2), 10 (TT3), or 15 (TT4) h at 150 °C. Then, they were slowly (0.5 °C/min) cooled to a crystallization temperature of 40 °C, where they were held for 5 h. Finally, they were quenched in liquid nitrogen. A reference sample (TT0) of each copolymer was prepared by holding the sample after solvent casting at 150 °C for only 3 min and cooling to −120 °C at 10 °C/min.

Transmission Electron Microscopy. Ultrathin sections (∼50 nm) of treated samples were cut at −120 °C using a Leica UCT ultramicrotome equipped with a diamond knife. Staining was achieved by treating the ultrathin sections for 50s with OsO_4 vapors under vacuum. Electron micrographs were taken with HITACHI H-500 and JEOL JEN 1220 microscopes, operating at 100 kV in the bright field mode.

SAXS/WAXS Experiments. SAXS/WAXS experiments were performed on station 8.2 at the synchrotron radiation source, Daresbury Laboratory, Daresbury, U.K. This instrument is configured with an X-ray wavelength $\lambda = 1.5$ Å. A 3.0 m camera was used for the SAXS data, recorded using a quadrant detector which gives a linear intensity profile as a function of wave vector. The wave vector scale was calibrated using a specimen of collagen (rat tail tendon). The data were corrected for the detector response. The WAXS data were recorded using a curved INEL position sensitive detector. Further details are provided elsewhere for the beamline[34] and the SAXS/WAXS/DSC instrument.[36]

Results and Discussion

In a previous work it was demonstrated that sample preparation conditions can strongly affect the thermal behavior of PS-*b*-PB-*b*-PCL triblock copolymers.[33] It was shown, for example, that the time the sample was annealed at 150 °C influences the melting behavior of the PCL block after isothermal crystallization at 40 °C. It was speculated that such behavior could be due to the confinement of lamellar crystals within nanostructures with varied long-range order and that, depending on composition, a "conflict" between microphase separation and crystallization can take place.[33] A summary of the previously determined thermal transitions of the copolymers used in the present study is shown in Table 2. In this table a trimodal ($S_{57}B_{27}C_{16}$) melting behavior and bimodal ($S_{51}B_{06}C_{40}$, $S_{25}B_{26}C_{49}$, $S_{27}B_{15}C_{58}$) melting behaviors for the PCL block are apparent for the samples subjected to the thermal treatments TT0, TT2, TT3, and TT4 described in the Experimental Part. With the exception of sample $S_{57}B_{27}C_{16}$, longer annealing times led to a general increase of the main melting point. This table also shows the Avrami parameters calculated from the isothermal crystallizations performed at 40 °C. In this work we try to correlate these results with the morphology of the samples investigated using transmission electron microscopy (TEM), polarized optical microscopy (POM), and synchrotron small-angle X-ray scattering (SAXS) experiments.

Before discussing TEM and SAXS results, it should be highlighted that the copolymers were microphase-separated at the temperature at which the annealing was performed (150 °C).[37,38]

It should also be mentioned that by using polarized optical microscopy no birefringence is observed at all for $S_{57}B_{27}C_{16}$. However, $S_{25}B_{26}C_{49}$ and $S_{51}B_{09}C_{40}$ exhibit, as can be observed in Figure 1, some granular superstructures that do not correspond to spherulites, since the typical extinction patterns are absent. Such textures can only be observed upon isothermal crystallizations of thin films (∼3 μm)[37] and are similar to the results found by Hong et al.[39,40] for PB-*b*-PEO diblock copolymers, indicating that the growth of crystallites propagates across grain boundaries in microphase-separated systems. $S_{27}B_{15}C_{58}$ is able, on the other hand, depending on preparation conditions, to form well-defined "banded" spherulites as will be discussed later.

Table 3 lists the Flory−Huggins parameters (χ_{12}) and interfacial tensions (γ_{12}) for the respective pairs in the PS-*b*-PB-*b*-PCL (SBC) triblock copolymers calculated from the middle Scott-Hildebrandt solubility parameters δ. A comparison among these values shows that the incompatibility increases in the serie PS/PCL ≪ PS/PB < PB/PCL. For this thermodynamic balance and the sequence $\phi_C < \phi_B < \phi_S$, i.e., the case where the S end block forms the matrix, the sum of the volume fractions

Table 2. Thermal Transitions Obtained for Treated and Untreated Block Copolymers[33]

sample	$T_{m(I)}$ (°C)	$T_{m(II)}$ (°C)	% X_m	n	sample	$T_{m(I)}$ (°C)	$T_{m(II)}$ (°C)	% X_m	n
$S_{57}B_{27}C_{16}$					$S_{25}B_{26}C_{49}$				
TT0	53.6	58.2	45		TT0	58.7		61	
TT2	54.7	61.1	54	1.82	TT2	60.5		62	1.73
TT3	55.2	61.2	62		TT3	61.5	47.9	65	
TT4[a]	55.7	61.1	59	2.03	TT4	61.5	43.9	65	1.78
$S_{51}B_{09}C_{40}$					$S_{27}B_{15}C_{58}$				
TT0	58.0		41		TT0	59.5		45	
TT2	58.2		54	1.98	TT2	61.4	35.1	63	4.05
TT3	59.8	39.1	59		TT3	62.2	40.5	66	
TT4	61.0	40.5	59	2.86	TT4	63.7	43.5	65	3.15

[a] A third melting endotherm was observed at 43.9 °C.

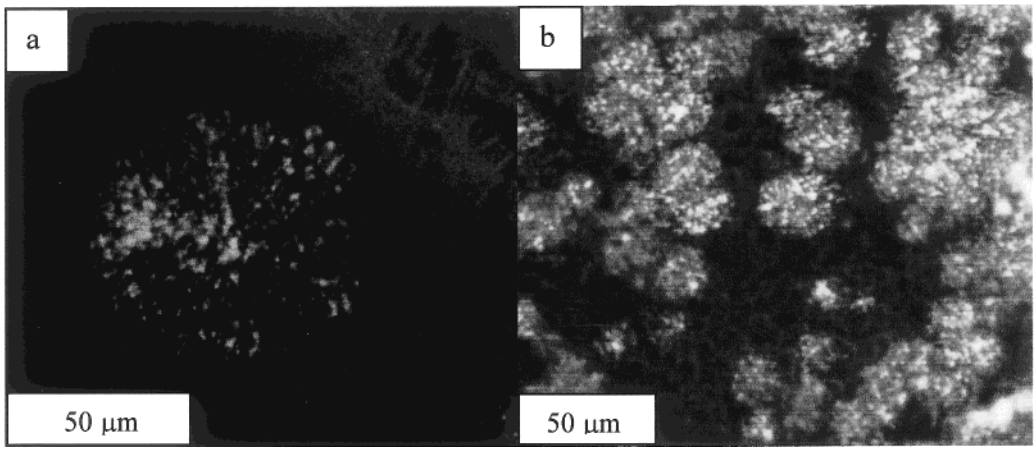

Figure 1. Polarizing optical micrographs of thin films of (a) $S_{25}B_{26}C_{49}$ and (b) $S_{51}B_{09}C_{40}$ crystallized isothermally at 44 and 42 °C, respectively. The samples were about 3 μm thick.

Table 3. Interaction Parameters (χ_{12}) and Interfacial Tensions (γ_{12}) of the SBC System[25]

polymer pair	PS/PB	PB/PCL	PS/PCL
χ_{12}	0.0623	0.1315	0.0118
γ_{12} (dyn·cm^{-1})	2.00	2.86	0.86

of the other components ($\phi_C + \phi_B$) will define whether a cylindrical or a spherical type morphology is formed.[41] Additionally, the ratio of the volume fractions ϕ_B/ϕ_C will control the type of cylindrical structure created.

For $S_{57}B_{27}C_{16}$, $\phi_C < \phi_B < \phi_S$ and $\phi_B/\phi_C = 2$; therefore, a cylindrical core−shell morphology is expected. In Figure 2, TEM micrographs of $S_{57}B_{27}C_{16}$ taken after the samples were annealed at 150 °C for 5 and 15 h are shown. In agreement with the similar melting points and degree of crystallinity obtained through DSC,[33] no significant changes are observed in the morphology. The morphology is similar to that previously reported by Balsamo et al.[25] with the formation of a dark PB shell around bright PCL cores in a PS matrix, as was predicted from the volume fractions and thermodynamic balance. Figure 3 shows a schematic representation of this cylinder in cylinder (c_ic) morphology. As illustrated, there seems to be a deformation of the cylinders which has been attributed to the presence of crystals (~54−62%) within them.[25] To estimate the dimensions of the microdomains shown in Table 4, we took the average from a perpendicular projection of the cylinders from many TEM micrographs. This morphology can unambiguously explain the fractionated crystallization exhibited by this copolymer ($T_{c(I)} = 30.5$ °C, $T_{c(II)} = -45.3$ °C).[25,33] Due to the low PCL content, this block builds a dispersed phase (cylinders), whose mean diameter is so small (see dimensions in Table 4) that the number of cylinders (10^{15} particles/cm^3) is much higher than the active heterogeneities normally present in a PCL homopolymer (10^7 particles/cm^3).[27] On the basis of the supercoolings observed in this block copolymer and on the glass transition of the PCL block (−65 °C), it can be ascertained that the fraction with the crystallization peak located at −45 °C emerges as a consequence of crystals that were homogeneously nucleated.

Table 4. TEM Microdomain Dimensions in $S_{57}B_{27}C_{16}$[a]

thermal treatment	D_{1S} (nm)	D_{2S} (nm)	D_{1C} (nm)	D_{2C} (nm)	L_{cic} (nm)
TT2	68.8 ± 1.0	35.9 ± 2.3	38.9 ± 3.9	13.7 ± 2.8	93.8 ± 8.8
TT3	71.0 ± 3.2	35.4 ± 2.9	41.7 ± 11.8	16.5 ± 3.2	88.2 ± 16.2
TT4	75.6 ± 8.1	46.4 ± 7.9	43.7 ± 12.6	15.0 ± 3.7	87.1 ± 14.6

[a] D_{1S}, D_{2S} = major and minor diameters of the PB shell, respectively. D_{1C}, D_{2C} = major and minor diameters of the PCL cores. L_{cic} = larger cylinder long period in the c_ic morphology.

The morphology formed upon crystallization of the PCL block after quenching to room temperature from the annealing temperature, and the microdomain structure in the melt, were investigated by SAXS for $S_{57}B_{27}C_{16}$. The most representative curves obtained during a heating scan of a sample TT4 are plotted in Figure 4. Although at room temperature, it was possible to identify the presence of core−shell cylinders by using TEM, we were not able to observe the expected sequence of high order reflections of this morphology in the SAXS curves below the melting temperature of the PCL block. This is probably due to the deformation of the microdomains caused by the presence of crystals within the cores. Crystallization of PCL was confirmed by WAXS patterns which contained Bragg reflections consistent with the orthorhombic unit cell.[42] However, in the melt, although the reflections are weak, the formation of a hexagonal packed cylinder structure is evident from the location of the higher order reflections.[43] Weak reflec-

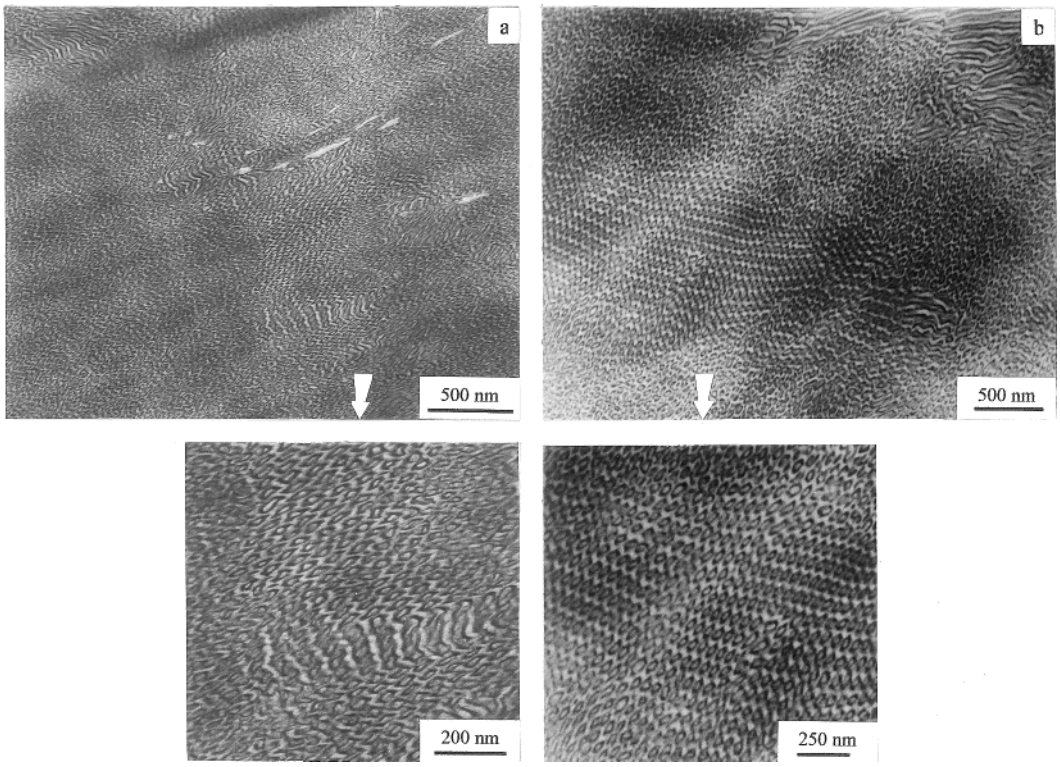

Figure 2. TEM images of $S_{57}B_{27}C_{16}$ after thermal treatments (a) TT2 and (b) TT4.

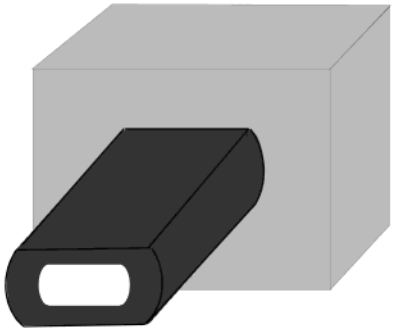

Figure 3. Schematic representation of the core−shell cylinders in the c_ic morphology for $S_{57}B_{27}C_{16}$.

tions are observed at q^* (0.0126 nm^{-1}), $\sqrt{3}q^*$ (0.0204 nm^{-1}) and $\sqrt{7}q^*$ (0.0304 nm^{-1}) (see arrows). Upon melting of the PCL block, a small increase of q^* is observed, especially above the PS glass transition. Over a range of 120 °C, q^* increases about 17%. Similar changes have been reported by other authors for semicrystalline diblock copolymers as well as for amorphous block copolymers[6,44−46] and result from a combination of changes in density, statistical segment length, and block incompatibility (reflected in χ changes) with temperature, which leads to a temperature dependent intercylinder spacing. The fact that the reflections, even in the melt, are not so marked may also be due to the relatively wide polydispersity of the samples (due to the PCL block synthesis).

The orientation of chain folds in semicrystalline block copolymers has been has been investigated by several groups mainly for polyethylene- (PE-) and poly(ethylene oxide)- (PEO-) based diblock copolymers. For asymmetric diblock copolymers with low molecular weights, where diffusion is rapid, the chain stems were found to be perpendicular to the cylinder axis. However, when chain mobility is limited, for example, at higher molecular weights or in diblocks with a glassy poly(vinylcyclohexane) PVCH block, chains are tilted with respect to the plane normal to the cylinder axis.[10] More recently, Cheng et al. reported that the tilt angle depends on crystallization temperature.[23] We did not perform orientation experiments in order to directly investigate the stem orientation. However, since $S_{57}B_{27}C_{16}$ exhibited fractionated crystallization, one can assume based on

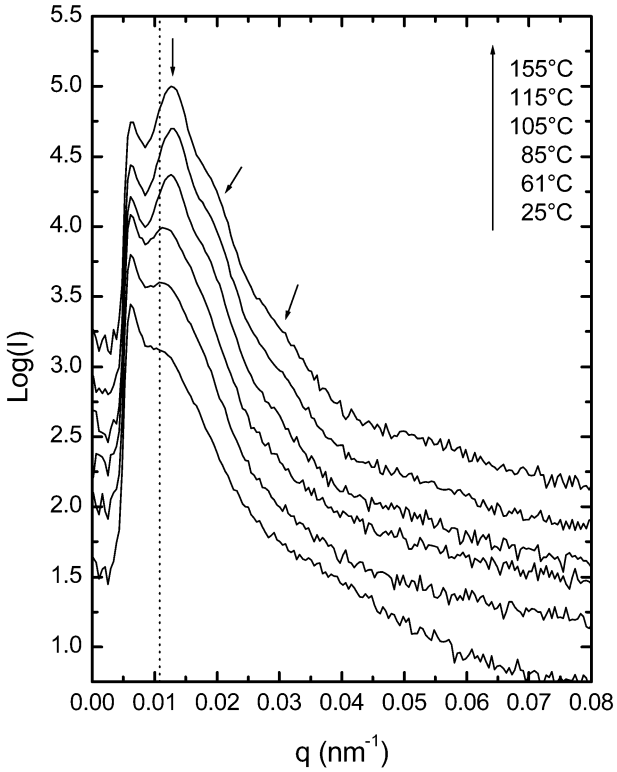

Figure 4. SAXS curves (logarithmic intensity scale) obtained for $S_{57}B_{27}C_{16}$ during a heating scan: bottom curve (25 °C); top curve (155 °C).

Table 5. TEM Microdomain Dimensions in $S_{51}B_{09}C_{40}$[a]

thermal treatment	L_{PCL} (nm)	L_{PS} (nm)	L_{lc} (nm)	D_{lc} (nm)	D_{PB} (nm)
TT2[a]	34.5 ± 2.4	25.8 ± 3.4	63.1 ± 9.8	17.7 ± 0.9	9.3 ± 0.7
thermal treatment	L_{PCL} (nm)	D_{PS} (nm)	L_{cr} (nm)	D_{ring} (nm)	D_{PB} (nm)
TT4[b]	–	24.3 ± 2.3	55.3 ± 3.9	15.5 ± 1.0	6.7 ± 1.2

[a] L_{PS}, L_{PCL} = thickness of the PS and PCL lamellae, respectively, L_{lc} = lamellar long period of lc morphology ($L_{lc} = L_{PCL} + L_{PS}$), D_{lc} = periodicity between cylinders, and D_{PB} = diameter of the PB cylinders. [b] D_{PS} = diameter of the PS cylinders, L_{cr} = cylinder long period of the cr morphology, D_{ring} = periodicity between rings, and D_{PB} = diameter of the PB rings.

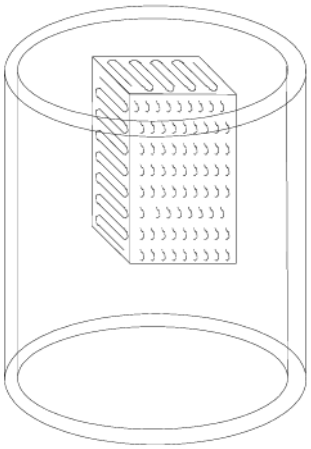

Figure 5. Schematic representation of the perpendicular orientation of PCL stems within core−shell cylinders.

the work of Cheng et al.[23] that those cylinders that were homogeneously nucleated present a random orientation of the crystallites, whereas those that were heterogeneously nucleated present a perpendicular orientation of the stems with respect to the microdomain interfaces as is depicted in Figure 5. Then, the small high melting temperature peak ($T_{m(II)}$ = 61 °C in Table 2) can be attributed to the melting of crystals that were heterogeneously nucleated at high temperature and the main melting peak ($T_{m(I)}$) at about 55 °C with a shoulder at ~43 °C ($T_{m(III)}$) to the crystals (~80% of the crystalline material) that were nucleated at low temperature, a fraction of which was probably homogeneously nucleated.[33] Such melting points correspond to approximate lamellar thicknesses of 8−10 nm.[47,48] Considering this and the crystallinity degree of 54−62%, one can assume, on the basis of the results presented in Table 2 and on the model shown in Figure 5, that only one crystallite of such dimensions can grow within a transversal plane of the cylinder. More layers would lead to the formation of thinner crystallites and to a higher depression of the melting temperature. Although Figure 5 shows a perfect perpendicular orientation of stems, we do not rule out that some tilting can occur. In fact, we have found evidence, in agreement with other authors, of such tilted orientation in a PS-*b*-PCL diblock copolymer by using atomic force microscopy.[48]

In contrast to $S_{57}B_{27}C_{16}$, copolymers with higher PCL content exhibit important changes by varying the annealing time at high temperature. Figure 6 shows TEM images of $S_{51}B_{09}C_{40}$ after annealing for 5 and 15 h at 140 °C. In Figure 6, parts a and b, PB can be unambiguously recognized as dark circular or ellipsoidal objects located at the interfaces of PS and PCL lamellae (lamellar−cylindrical (lc) morphology). Because of the regularity of these objects at the interfaces, they have been interpreted as PB cylinders. Because the ultrathin section is not always perpendicular to the cylinder direction, the PB cylinder cross sections appear sometimes as ellipses (see Figure 7a).[49,50] In addition, the electron micrographs show that cylinders in successive layers are directly opposed. Depending on the microtoming direction relative to the orientation of different lamellar stacks, variable thicknesses can be obtained from the TEM images. To obtain the most appropriate long period, the smallest dimensions were taken. These dimensions are summarized in Table 5. When this copolymer was annealed for 15 h, a change in the morphology occurred as can be appreciated in Figure 6, parts c and d. The micrographs shows transversal sections of PS cylinders as well as PS cylinders, which were cut parallel to their main axis. One can also clearly recognize the presence of very small dark structures around the transverse section of the cylinders (arrow 1) along with very small dark structures located along the cylinders that were cut parallel to their main axis (arrow 2). On the basis of the extremely regular arrangement, we have to conclude that the PB midblock forms small isolated rings surrounding the PS cylinders in the PCL matrix as is schematically shown in Figure 7b. As an example, this figure illustrates the formation of six dark objects around the PS cylinders as a consequence of the cutting angle. This morphology, reported by Stadler et al. for a polystyrene-*b*-poly(ethylene-*co*-butylene)-*b*-poly(methyl methacrylate) $S_{45}EB_{06}M_{49}$ has been described as a cylinder−ring (cr) morphology.[49,50] Taking into account the volume fractions of the components and that $\gamma_{AB} < \gamma_{BC}$, $\gamma_1 = \gamma_{BC}/\gamma_{AB}$ (1.43), $\gamma_2 = \gamma_{AC}/\gamma_{AB}$ (0.43), from the theory,[50,51] a lamellar-spherical or a lamellar−cylindrical morphology for this composition should be expected (PS and PCL lamellae with PB spheres or cylinders located at the interfaces). Although the sample annealed for 5 h exhibited the expected morphology, after 15 h annealing, when it can be supposed that a higher equilibration of the morphology has been reached, a cr morphology was obtained. This type of transition has only been reported upon hydrogenation of the PB middle block in polystyrene-*b*-polybutadiene-*b*-poly(methyl methacrylate) triblock copolymers.[50] It was attributed to the change of the Flory−Huggins interaction parameters with the chemical modification, which leads to a higher asymmetric incompatibility of the middle block with the outer blocks.[49,50] Since we observed neither changes in the glass transitions of the components nor chemical degradation, we cannot explain yet the reason for such a transition in $S_{51}B_{09}C_{40}$, but it is known that such a morphological transition can occur as a means to reduce the contacts between the C and B blocks.[50]

Cross sections (~3 μm) of treated samples of $S_{51}B_{09}C_{40}$ were cut using a microtome at liquid nitrogen temperature. Under polarizing light in an optical microscope, we could not distinguish, even in the sample with a PCL matrix (TT4), the presence of spherulites. This is in agreement with calculated Avrami parameters lower

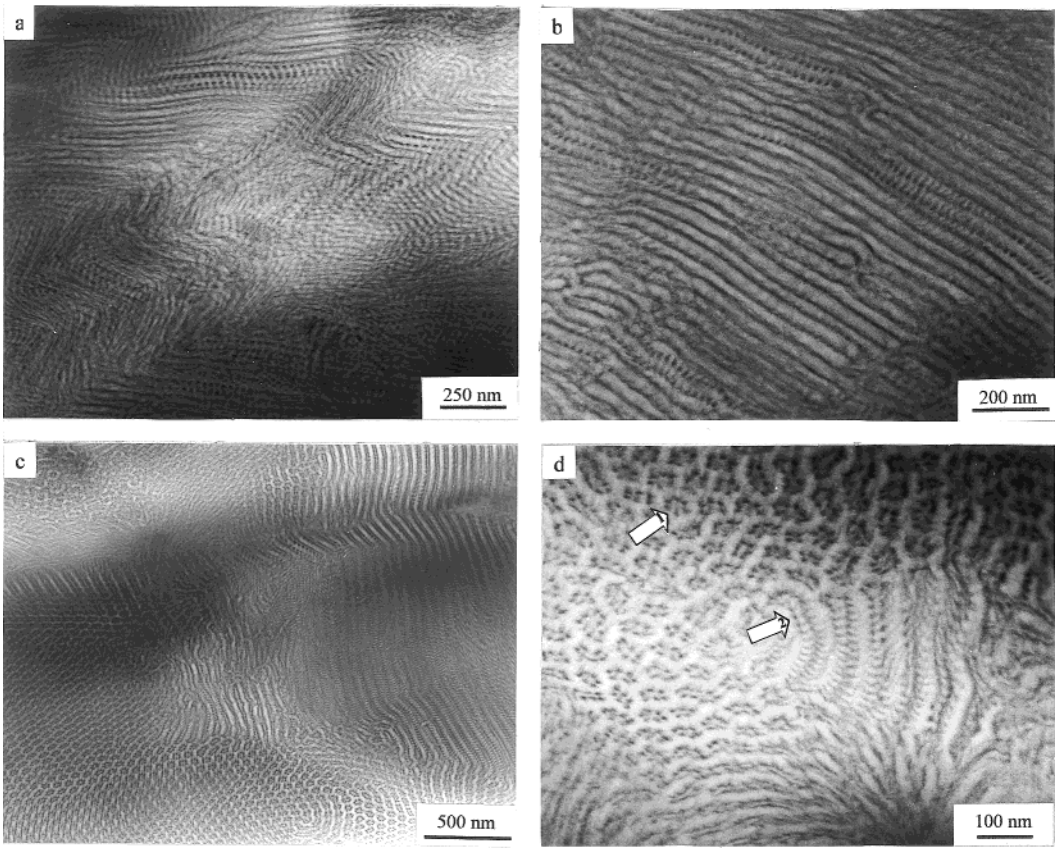

Figure 6. TEM images of $S_{51}B_{09}C_{40}$ after thermal treatments (a, b) TT2 and (c, d) TT4.

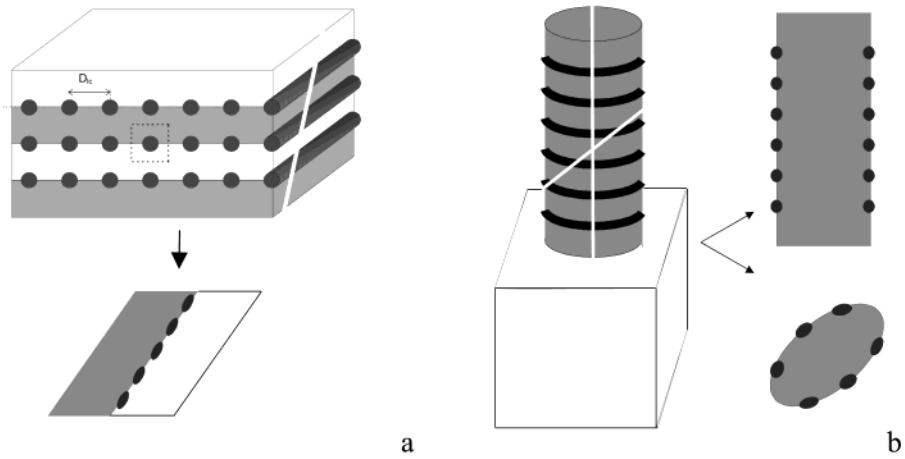

Figure 7. Schematic representation of the (a) lamellar−cylindrical (lc) and (b) cylinder−ring (cr) morphologies for $S_{51}B_{09}C_{40}$ TT2 and TT4, respectively. Black regions are PB, gray regions are PS, and white regions are PCL.

than 3 shown in Table 2[33] and with the results of Register et al.[52] These authors found that even a polystyrene-*b*-polyethylene diblock copolymer with 80 wt % PS can retain its hexagonally packed cylindrical morphology formed in the melt upon crystallization producing an induced orientation of the PE crystals that form between the cylinders. However, as mentioned at the beginning of this discussion, $S_{51}B_{09}C_{40}$ is able to build a superstructure when the crystallization proceeds from thin films. This is also in agreement with the results of Jackson et al.,[32] who found that a $S_{35}B_{15}C_{50}$ triblock copolymer was able to build spherulites in thin films, but not from the bulk, when a clear microphase separation was developed. The formation of such textures on crystallization in microphase-separated systems has also been reported by Hong et al.,[39,40] who suggested that crystallization can propagate through grain boundaries and can propagate to encompass many differently oriented grains. This is possible due to the grain boundary morphologies in microphase-separated lamellar systems which provide for continuity of domain structure across the boundaries. Nevertheless, as we will show below in the discussion of the morphology of $S_{27}B_{15}C_{58}$, the coexistence of spherulites with a well-developed microdomain morphology is also possible.

On the basis of the above discussion and the absence of spherulites in $S_{51}B_{09}C_{40}$ TT4, it is concluded that 9% PB does not give the system enough mobility to destroy the previous melt mesophase due to the relatively high content of the PS block.

Table 2 shows that the melting points exhibited by $S_{51}B_{09}C_{40}$ increase from 58.2 to 61.0 °C for samples TT2

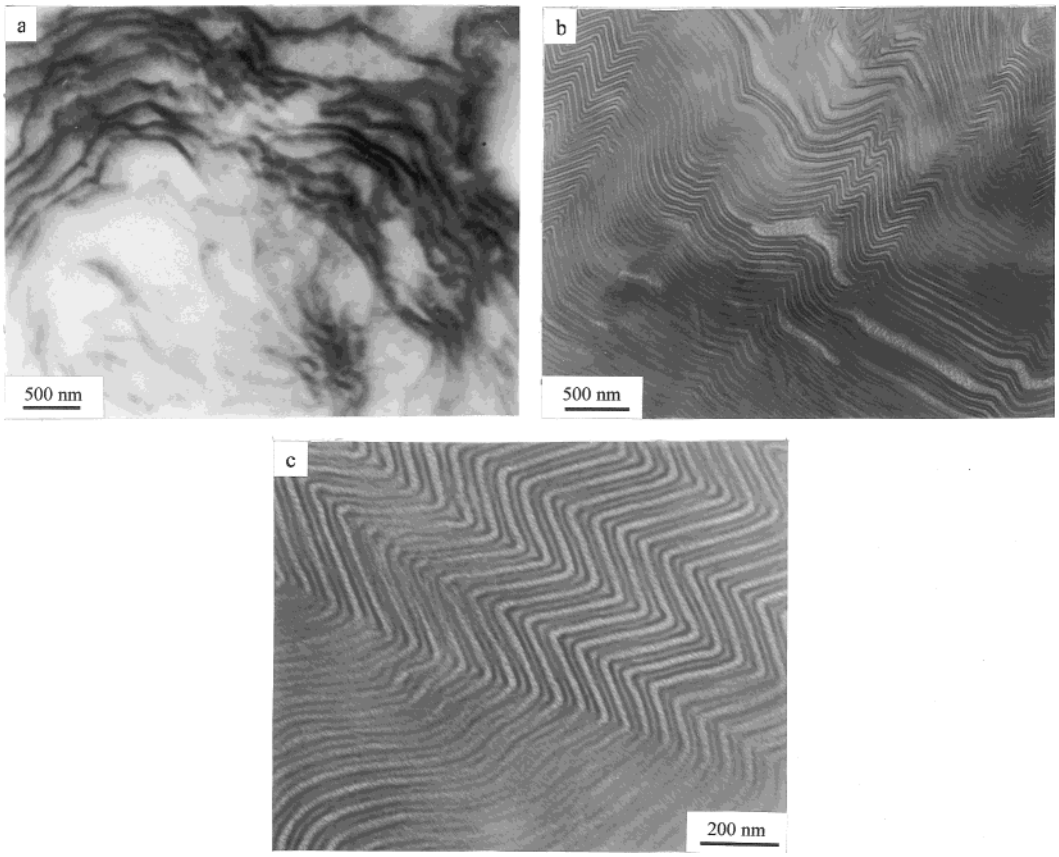

Figure 8. TEM images of $S_{25}B_{26}C_{49}$ after thermal treatments (a) TT2 and (b, c) TT4.

and TT4, respectively. Such a slight increase can be attributed to the higher freedom for crystalline lamellae thickening in TT4, due to the fact that in this sample the PCL forms the matrix. Although in sample TT2 the PCL block is confined in lamellae, it did not exhibit fractionated crystallization. This suggests the formation of interconnected lamellae as is shown by the arrow in Figure 6b.

Figure 8 shows TEM micrographs of $S_{25}B_{26}C_{49}$. It can be clearly observed that the morphology changes dramatically as the annealing time is increased. Interestingly, when this sample has been annealed only for 5 h (Figure 8a), it does not show a clear microphase separation. This could indicate that initially mixing took place between some of the components during film preparation. Nevertheless, the glass transitions of the three components could be unambiguously determined through DSC ($T_{gPB} = -96.6$ °C, $T_{g\ PCL} = -62.2$ °C, and $T_{g\ PS} = 94.9$ °C).[33] After 15 h of annealing (Figure 8, parts b and c), on the other hand, a very well-defined lamellar−lamellar (ll) morphology is formed as expected from the volume fractions and interaction parameters. A strong influence of the annealing time on the morphology developed by block copolymers has been reported before.[53] However, it is important to note that this effect will depend on the relative free energy difference among different structures and the activation energy required for morphological rearrangements, which will depend on copolymer composition. Figure 8 shows a micrograph for a copolymer for which an annealing time of 5 h is not enough to generate an ordered morphology. This behavior seems to be reproducible for polystyrene-*b*-polybutadiene-*b*-poly(ϵ-caprolactone) triblock copolymers containing more than 25% of PB and less than 30% PS, i.e., when the total volume fraction of low T_g components ($\phi_B + \phi_C$) is higher than 0,7.[36,49] This means that the incompletely developed morphology at low annealing times is trapped on cooling. However, when the melt morphology has been equilibrated at larger annealing times, it is frozen with the help of the minority glassy block, resulting in a clear microphase-separated morphology.

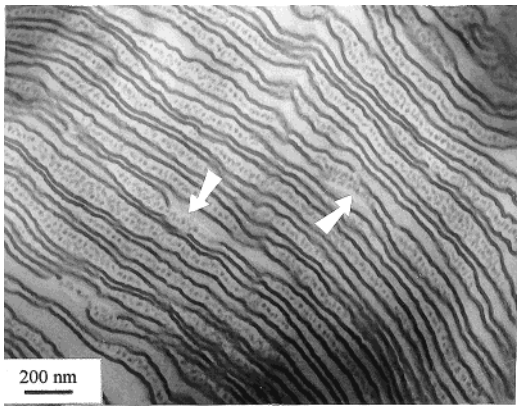

Figure 9. TEM image of $S_{25}B_{26}C_{49}$ after thermal treatment TT3.

To investigate an intermediate situation between an annealing for 5 and 15 h in $S_{25}B_{26}C_{49}$ a sample that was annealed for 10 h was analyzed by TEM. Figure 9 shows a lamellar-like structure with some peculiar features. In some regions of the image, the PB block forms dark lamellae whose thickness is ~13 nm (see Table 6) and in other regions spherical dark domains. This image represents a metaestable morphology in which the formation of PB lamellae is probably taking place from PB spheres (see arrows in Figure 9 and a schematic representation in Figure 10). Although its origin remain

Table 6. TEM Microdomain Dimensions in $S_{25}B_{26}C_{49}$[a]

thermal treatment	L_{PB} (nm)
TT3[a]	13.4 ± 1.3

thermal treatment	L_{PS} (nm)	L_{PB} (nm)	L_{PCL}m)	L_{II} (nm)
TT4[b]	12.1 ± 1.1	11.4 ± 0.9	22.9 ± 1.7	57.1 ± 4.1

[a] L_{PB} = thickness of the PB lamella. [b] L_{II} = lamellar long period of the ll morphology ($L_{II} = L_{PS} + 2L_{PB} + L_{PCL}$); L_{PS}, L_{PB}, L_{PCL} = thickness of the PS, PB and PCL lamellae, respectively.

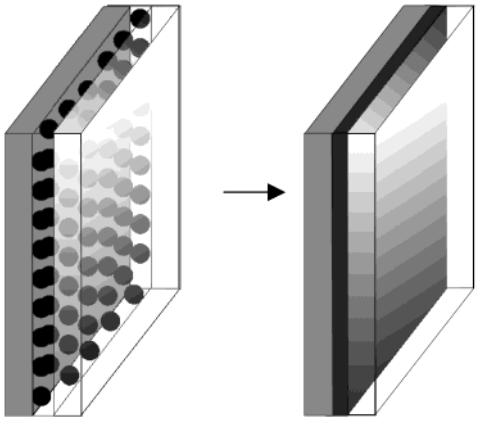

Figure 10. Schematic representation of the formation of PB lamellae from PB spheres.

unclear, it resembles in some way the epitaxial relationship reported by other authors[8,12] between hexagonal melt and lamellar solid phases.

The highly ordered microstructure obtained for $S_{25}B_{26}C_{49}$ after 15 h of annealing led us to assume that, although they contain 49% PCL, these samples would not form spherulites. Therefore, using a microtome, we cut sections of the treated samples of about 3 μm thickness for observation in the optical microscope under polarizing light. No spherulitic superstructure was observed. This is in agreement with the reported Avrami exponent $n = 1.78$ for this copolymer (see Table 2). However, as mentioned before, Jackson et al.[32] demonstrated that the observation of superstructures in these ABC triblock copolymers in the optical microscope depends a lot on the thickness of the sample. Accordingly, when crystallization took place directly from the melt in very thin films, some coarse spherical superstructures were observed (see Figure 1), which exhibited a linear radial growth with time.[36]

The final copolymer we examined is $S_{27}B_{15}C_{58}$, which also exhibits a complex behavior. Balsamo et al. have reported that this copolymer is able to form spherulites when crystallization takes place isothermally or during a cooling scan in thin films (3−5 μm).[24] Simultaneously, a lamellar−lamellar morphology was observed by TEM for samples that were cryogenically cut from 1 mm thick specimens.[29] Then, the question arises how such lamellar microdomains could be arranged within spherulites. The presence of spherulites indicates that crystalline stems are oriented perpendicular to the interfaces in order to make possible the radial lamellar growth from a nucleating center. Nevertheless, as mentioned before, it has been demonstrated that stem orientation depends on crystallization temperature.[22,23] Thus, the relationship between crystallization and microphase separation is very complex, because not only the segregation level and the glass transition of the amorphous blocks but also crystallization conditions can affect stem orientation. In our case the triblock copolymers under study have a crystallizable block that is covalently linked to a rubbery block at the crystallization temperature, but at the same time, there is a glassy block that could disturb the crystallization process. Within a lamellar−lamellar morphology, a parallel stem orientation would limit the lateral growth of the crystal by the microdomain width, but its thickness could be more easily increased. Conversely, with a perpendicular stem orientation the crystalline lamellae can grow laterally, but the lamellar thickening is more limited.

Table 7. TEM Microdomain Dimensions in $S_{27}B_{15}C_{58}$

$S_{27}B_{15}C_{58}$	L_{PS} (nm)	L_{PB} (nm)	L_{PCL} (nm)	L_{II} (nm)
TT2	24.6 ± 2.0	15.1 ± 1.3	30.2 ± 2.1	90.2 ± 7.2
TT3	21.2 ± 1.8	15.1 ± 1.2	30.1 ± 2.0	87.7 ± 6.8
TT4	25.5 ± 2.1	15.1 ± 1.2	30.1 ± 2.0	90.2 ± 7.0

[a] L_{PS}, L_{PB}, L_{PCL} = thicknesses of the PS, PB, and PCL lamellae, respectively. L_{II} = lamellar long period of the ll morphology ($L_{II} = L_{PS} + 2L_{PB} + L_{PCL}$).

To investigate the relationship between microphase separation and spherulite formation, we present TEM images of $S_{27}B_{15}C_{58}$ in Figure 11. Taking into account the volume fractions of the components, a lamellar−cylindrical morphology is expected. However, as was previously reported, this copolymer exhibits a lamellar−lamellar morphology.[29] A tendency for semicrystalline block copolymers to form lamellar morphologies has been shown by other authors for semicrystalline diblock copolymers.[4] Despite the unambiguous assignment of the morphology (lamellar−lamellar), the SBC triblock copolymer annealed for only 5 h shows a reduced long-range order with respect to the sample annealed for 15 h, with presence in the TEM image of more curved lamellae and defects. Sections of these samples of about 3 μm thickness were investigated in the optical microscope. Interestingly, the sample annealed for 5 h exhibited banded spherulites (see Figure 12), whereas the sample annealed for 15 h did not. This copolymer does not show significant changes in microdomain spacings for different thermal treatments (Table 7), but it does exhibit important variations in its thermal behavior (Table 2). Then, we suggest that at moderately high PCL contents, where lamellar−lamellar microphases are formed, the order reached in the melt could define the orientation of the stems on crystallization. Long-range ordered morphologies seem to generate a parallel stem orientation with the absence of spherulites. On the other hand, poorly ordered morphologies appear to lead to a perpendicular stem orientation and spherulite formation. This is in agreement with the calculated Avrami exponents. The value for the sample annealed for 5 h and crystallized at T_c = 40 °C was 4.05, indicating a three-dimensional growth, in which the nucleation step is mainly sporadic. On the other hand, in the sample annealed for 15 h, the Avrami parameter decreased to 3.15, which suggests a bidimensional growth combined with a sporadic nucleation.

Therefore, the "conflict" between microphase separation and spherulite formation is clear for the $S_{27}B_{15}C_{58}$ triblock copolymer. The melting temperature of this copolymer changes from 61.4 to 63.7 °C within lamellae that have approximately the same dimensions. Such an increase can be explained because, as mentioned above, a parallel stem orientation would allow the crystals to thicken with fewer restrictions. This is in agreement with Nojima et al., in the sense that the slight changes

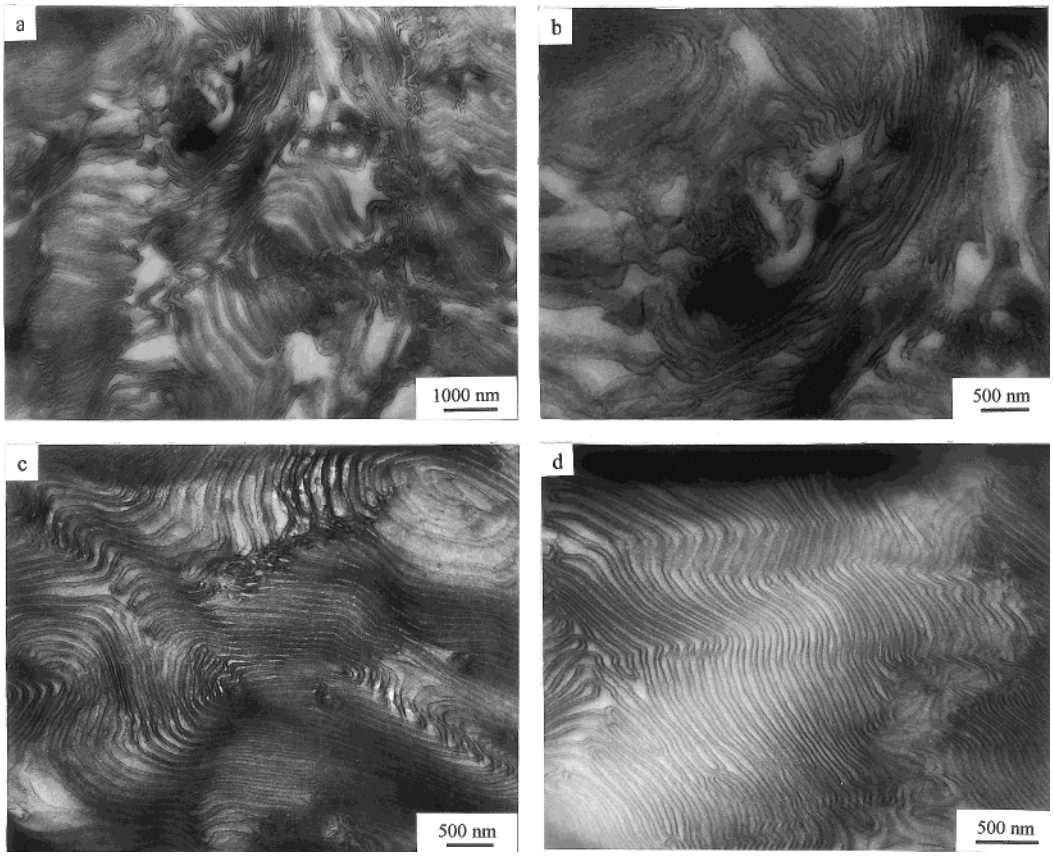

Figure 11. TEM images of $S_{27}B_{15}C_{58}$ after thermal treatments (a, b) TT2 and (c, d) TT4.

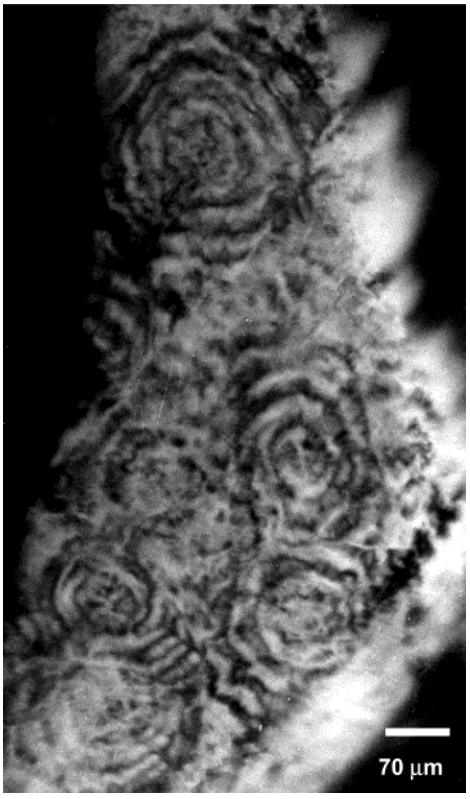

Figure 12. Polarized optical micrograph of 3 μm sections of $S_{27}B_{15}C_{58}$ TT4.

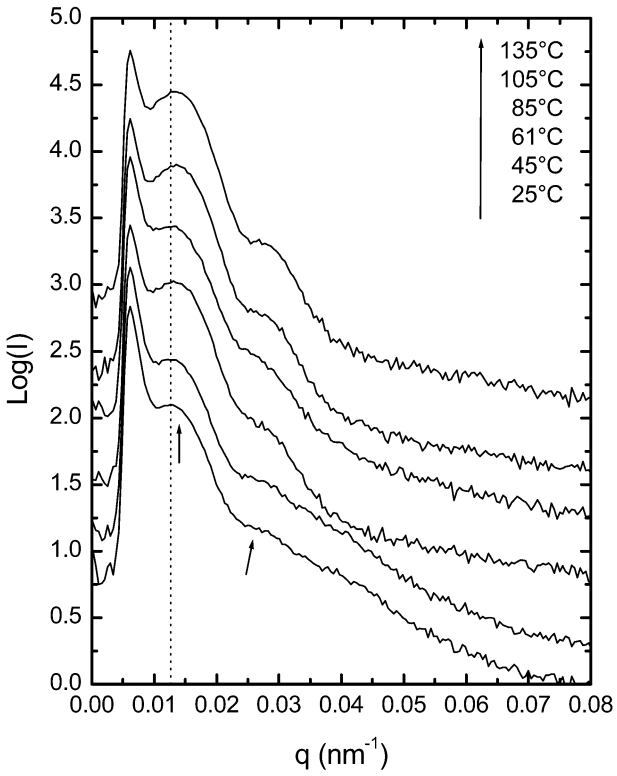

Figure 13. SAXS curves (logarithmic intensity scale) obtained for $S_{27}B_{15}C_{58}$ during a heating scan: bottom curve (25 °C); top curve (135 °C).

in the thermal behavior are due to the internal structure of the lamellar crystals in the PCL domains.

Representative SAXS curves obtained during a heating scan of $S_{27}B_{15}C_{58}$ TT4 are plotted in Figure 13. Initially, at room temperature, two reflections are observed centered at q^* and $2q^*$ (see arrows), corresponding to a lamellar−lamellar morphology as was demonstrated by TEM. No higher-order SAXS peak was

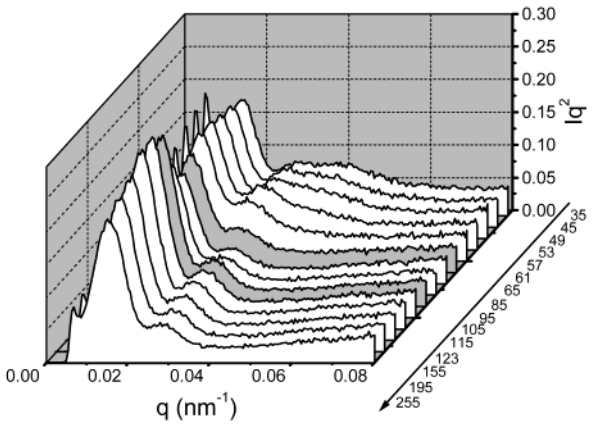

Figure 14. Iq^2 vs q for $S_{27}B_{15}C_{58}$ obtained during a heating scan from 25 to 255 °C. The filled curves correspond to 61 and 105 °C, respectively.

observed from the lamellar−lamellar morphology, which may be attributed to the long-range order level reached and/or polydispersity of the copolymer. The repeat distance obtained from these curves corresponds to 79 nm, which is somewhat smaller than the dimensions measured from TEM images, since the dimensions taken from TEM images can be overestimated due to the different cutting angles. In addition, a broad hump is observed at about 0.043 nm^{-1}, whose intensity is reduced progressively up to the PCL melting temperature, indicating that it is caused by scattering from PCL crystallites. From Figure 13, it can be also observed that upon melting only a small increase of q^* from 0.0126 to 0.0131 nm^{-1} is observed. Therefore, upon melting, the lamellar−lamellar morphology is preserved even up to temperatures as high as 255 °C (see Figure 14), where degradation of the copolymer takes place. The observed small increase of q^* indicates a decrease of the interlamellar spacing as is expected from melting of the crystals. Changes in intensity can be better appreciated in Figure 14 in the 25−255 °C temperature range. Upon melting, there is a decrease of intensity, followed by an increase up to 130 °C, where the instensity begins again to diminish.

Conclusions

The interplay between microphase morphology and thermal behavior was investigated following crystallization in a series of polystyrene-*b*-polybutadiene-*b*-poly(ϵ-caprolactone) ABC triblock copolymers as a function of the annealing time at high temperature, keeping the crystallization conditions identical. It was demonstrated that in highly confined PCL microdomains like cylinders, the number of microdomains is much higher than the active heterogeneities usually present in a PCL homopolymer, so that homogeneous nucleation can take place. Nevertheless, the coexistence of homogeneous and heterogeneous nucleation in $S_{57}B_{27}C_{16}$ suggests that some of the cylinders are interconnected.

In contrast to $S_{57}B_{27}C_{16}$, copolymers with higher PCL contents exhibited pronounced changes by varying the annealing time at high temperature. A copolymer like $S_{51}B_{09}C_{40}$ experiences a morphological transition from a lamellar−cylindrical (lc) to a cylindrical−ring (cr) morphology as a means to reduce the contacts between the C and B blocks. Despite the relatively high PCL contents, this copolymer is not able to form spherulitic superstructures, in agreement with the Avrami exponent. However, it can be concluded that a clear microphase separation does not always prevent the formation of spherulites, since a copolymer like $S_{27}B_{15}C_{58}$ showed formation of spherulites with a well-developed microdomain morphology. Nevertheless, it can be ascertained that within a well-developed microdomain morphology, the extent of long-range order influences the "conflict" between microphase separation and crystallization that can be related to the melting temperature and Avrami parameters associated with the crystallization kinetics. Thus, within a copolymer, the formation of spherulites is inhibited if a long-range ordered morphology is attained, with a resulting higher melting point probably due to a change in the crystalline stem orientation.

An extreme situation was represented by $S_{25}B_{26}C_{49}$, in which the annealing time produced a dramatic morphological change from a disordered to a well-developed lamellar−lamellar morphology being this behavior seem to be reproducible for copolymers in which the total volume fraction of the low T_g components ($\phi_B + \phi_C$) is higher than 0.7.

Acknowledgment. This work was made possible by the financial support of the "Fondo Nacional de Ciencia, Tecnología e Innovación" (FONACIT) through Grant F-95000716 and of the "Decanato de Investigación y Desarrollo" from Simón Bolívar University through Grant DID-G02.

References and Notes

(1) Rangarajan, P.; Register, R. A.; Fetters, L. J. *Macromolecules* **1993**, *26*, 4640.
(2) Nojima, S.; Nakano, H.; Takahashi, Y.; Ashida, T. *Polymer* **35**, **1994**, *16*, 3479.
(3) Rangarajan, P.; Register, R. A.; Fetters, L. J.; Naylor, S.; Ryan, A. J. *Macromolecules* **1995**, *28*, 1422.
(4) Ryan, A. J.; Hamley, I. W.; Bras, W.; Bates, F. S. *Macromolecules* **1995**, *28*, 3860.
(5) Nojima, S.; Hashizume, K.; Rohadi, A.; Sasaki, S. *Polymer* **38**, **1997**, *11*, 2711.
(6) Quiram, D. J.; Register, R. A.; Marchand, G. R.; Ryan, A. J. *Macromolecules* **1997**, *30*, 8338.
(7) Quiram, D. J.; Register, R. A.; Marchand, G. R.; Ryan, A. J. *Macromolecules* **1997**, *30*, 4551.
(8) Ryan, A. J.; Fairclough, J. P. A.; Hamley, I. W.; Mai, S. M.; Booth, C. *Macromolecules* **1997**, *30*, 1723.
(9) Hamley, I. W.; Fairclough, J. P. A.; Ryan, A. J.; Bates, F. S.; Towns-Andrews, E. *Polymer* **1996**, *37*, 4425.
(10) Quiram, D. J.; Register, R. A.; Marchand, G. R.; Adamson, D. H. *Macromolecules* **1998**, *31*, 4891.
(11) Weimann, P. A.; Hajduk, D. A.; Chu, C.; Chaffin, K. A.; Brodil, J. C.; Bates, F. S. *J. Polym. Sci., B: Polym. Phys.* **1999**, *37*, 2053.
(12) Hamley, I. W.; Fairclough, J. P. A.; Terrill, N. J.; Ryan, A. J.; Lipic, P. M.; Bates, F. S.; Towns-Andrews, E. *Macromolecules* **1996**, *29*, 8835.
(13) Zhu, L.; Cheng, S. Z. D.; Calhoun, B. H.; Ge, Q.; Quirk, R. P.; Thomas, E. L.; Hsiao, B. S.; Yeh, F. J.; Lotz, B. *J. Am. Chem. Soc.* **2000**, *122*, 5927.
(14)) Loo, Y. J.; Register, R. A.; Ryan, A. J. *J. Phys. Rev. Lett.* **2000**, *84*, 4120.
(15) Loo, Y. L.; Register, R. A.; Ryan, A. J.; Dee, G. T. *Macromolecules* **2001**, *34*, 8968.
(16) Lotz, B.; Kovacs, A. J. *Kolloid Z. Z. Polym.* **1966**, *209*, 97.
(17) Lotz, B.; Kovacs, A. J.; Bassett, G. A.; Keller, A. *Kolloid Z. Z. Polym.* **1966**, *209*, 115.
(18) Kovacs, A. J.; Lotz, B.; Keller, A. *J. Macromol. Sci. Phys.* **1969**, *B3* (3), 385.
(19) Hirata, E.; Ijitsu, T.; Hashimoto, T.; Kawai, H. *Polymer* **1975**, *16*, 249.
(20) Yang, Y. W.; Tanodekaew, S.; Mai, S. M.; Booth, C.; Ryan, A. J.; Bras, W.; Viras, K. *Macromolecules* **1995**, *26*, 6029.
(21) Cohen, R. E.; Bellare, L.; Drzewinski, M. A. *Macromolecules* **1994**, *27*, 2321.

(22) Zhu, L.; Calhoun, B. H.; Ge, Q.; Quirk, R. P.; Cheng, A. Z. D.; Thomas, E. L.; Hsiao, B. S.; Yeh, F.; Liu, L.; Lotz, B. *Macromolecules* **2001**, *34*, 1244.
(23) Huang, P.; Zhu, L.; Cheng, S. Z. D.; Ge, Q.; Quirk, R. P.; Thomas, E. L.; Lotz, B.; Hsiao, S.; Liu, L.; Yeh, F. *Macromolecules* **2001**, *34*, 6649.
(24) Balsamo, V.; von Gyldenfeldt, F.; Stadler, R. *Macromol. Chem. Phys.* **1996**, *197*, 3317.
(25) Balsamo, V.; von Gyldenfeldt, F.; Stadler, R. *Macromolecules* **1999**, *32*, 1226.
(26) Balsamo, V.; Müller, A. J.; von Gyldenfeldt, F.; Stadler, R. *Macromol. Chem. Phys.* **1998**, *199*, 1063.
(27) Müller, A. J.; Balsamo, V.; Arnal, M. L.; Jakob, T.; Schmalz, H.; Abetz, V. *Macromolecules* **2002**, *35*, 3048.
(28) Arnal, M. L.; Balsamo, V.; López-Carrasquero, F.; Contreras, J.; Carrillo, M.; Schmalz, H.; Abetz, V.; Laredo, E.; Müller, A. J. *Macromolecules* **2001**, *34*, 7973.
(29) Balsamo, V.; Stadler, R. *Macromolecules* **1999**, *32*, 3994.
(30) Balsamo, V.; Stadler, R. *Macromol. Symp.* **1997**, *117*, 153.
(31) Bailey, T. S.; Pham, H. D.; Bates, F. S. *Macromolecules* **2001**, *34*, 6994.
(32) Kim, G.; Han, C. C.; Libera, M.; Jackson, C. L. *Macromolecules* **2001**, *34*, 7336.
(33) Balsamo, V.; Gil, G.; Urbina de Navarro, C. *Macromolecules*, in press.
(34) Balsamo, V.; von Gyldenfeldt, F.; Stadler, R. *Macromol. Chem. Phys.* **1996**, *197*, 1159.
(35) Bras, W.; Derbyshire, G. E.; Ryan, A. J.; Mant, G. R.; Felton, R. A.; Lewis, R. A.; Hall, C. J.; Greaves, G. N. *Nucl. Instrum. Methods Phys. Res. A* **1993**, *326*, 587.
(36) Bras, W.; Derbyshire, G. E.; Cedie, J.; Komanschek, B. U.; Devine, A.; Clark, S. M.; Ryan, A. J. *J. Appl. Crystallogr.* **1995**, *28*, 26.
(37) Balsamo, V. Ph.D. Thesis, University of Mainz, 1996.
(38) von Gyldenfeldt, F. Ph.D. Thesis, University of Bayreuth, 1999.
(39) Hong, S.; MacKnight, W. J.; Russell, T. P.; Gido, S. P. *Macromolecules* **2001**, *34*, 2876.
(40) Hong, S.; Yang, L.; MacKnight, W. J.; Gido, S. P. *Macromolecules* **2001**, *34*, 7009.
(41) Breiner, U.; Krappe, U.; Abetz, V.; Stadler, R. *Macromol. Chem. Phys.* **1997**, *198*, 1051.
(42) Chatani, Y.; Okita, Y.; Tadokoro, H.; Yamashita, Y. *Polym. J.* **1970**, *1*, 552.
(43) Hamley, I. W. *The Physics of Block Copolymers*; Oxford University Press: New York, 1998.
(44) Sakurai, S.; Hashimoto, T.; Fetters, L. J. *Macromolecules* **1995**, *28*, 7947.
(45) Sakamoto, N.; Hashimoto, T. *Macromolecules* **1995**, *28*, 6825.
(46) Rosedale, J. H.; Bates, F. S.; Almdal, K.; Mortensen, K.; Wignall, G. D. *Macromolecules* **1995**, *28*, 1429.
(47) Balsamo, V.; Collins, S.; Hamley, I. W. *Polymer* **2002**, *43*, 15, 4207.
(48) Balsamo, V.; Collins, S.; Hamley, I. W. Manuscript in preparation.
(49) Auschra, C.; Stadler, R. *Macromolecules* **1993**, *26*, 2171.
(50) Stadler, R.; Auschra, C.; Beckmann, J.; Krappe, U.; Voigt-Martin, I.; Leibler, L. *Macromolecules* **1995**, *28*, 3080.
(51) Zheng, W.; Wang, Z. G. *Macromolecules* **1995**, *28*, 7215.
(52) Loo, Y. L.; Register, R. A.; Adamson, D. H. *Macromolecules* **2000**, *33*, 8361.
(53) Vigild, M. E.; Almdal, K.; Mortensen, K.; Hamley, I. W.; Fairclough, F. P. A.; Ryan, A. J. *Macromolecules* **1998**, *31*, 5702.
(54) Balsamo, V.; von Gyldenfeldt, F.; Jakob, T.; Abetz, V. To be published.

MA020129O